



HAL
open science

Modeling the seismic signature of structural data from the Oman Ophiolite: Can a mantle diapir be detected beneath the East Pacific Rise?

David Jousselin, Robert Dunn, Douglas R. Toomey

► **To cite this version:**

David Jousselin, Robert Dunn, Douglas R. Toomey. Modeling the seismic signature of structural data from the Oman Ophiolite: Can a mantle diapir be detected beneath the East Pacific Rise?. *Geochemistry, Geophysics, Geosystems*, 2003, 4 (7), 10.1029/2002GC000418 . hal-02374836

HAL Id: hal-02374836

<https://hal.science/hal-02374836>

Submitted on 21 Nov 2019

HAL is a multi-disciplinary open access archive for the deposit and dissemination of scientific research documents, whether they are published or not. The documents may come from teaching and research institutions in France or abroad, or from public or private research centers.

L'archive ouverte pluridisciplinaire **HAL**, est destinée au dépôt et à la diffusion de documents scientifiques de niveau recherche, publiés ou non, émanant des établissements d'enseignement et de recherche français ou étrangers, des laboratoires publics ou privés.



Modeling the seismic signature of structural data from the Oman Ophiolite: Can a mantle diapir be detected beneath the East Pacific Rise?

David Jouselin

Department of Geological Sciences, University of Oregon, Eugene, Oregon 97403, USA

*Now at INPL/ENSG-CRPG, 15 rue Notre Dame des Pauvres, 54501 Vandoeuvre-les-Nancy, France.
(jousse@crpg.cnrs-nancy.fr)*

Robert Dunn

Department of Geology and Geophysics, University of Hawaii, Honolulu, Hawaii 96822, USA

Douglas R. Toomey

Department of Geological Sciences, University of Oregon, Eugene, Oregon 97403, USA

[1] We present modeling of the seismic delay time signature of mantle diapirs mapped in the Oman ophiolite and compare these results with those of active source seismic experiments conducted along the East Pacific Rise. To do so, we construct models of shallow-mantle, seismic anisotropy that are consistent with Oman diapirs of different size. Forward calculations of the delay time anomalies due to a combination of diapir-related seismic anisotropy and isotropic velocity structure are compared with those of a two-dimensional anisotropy field within the same isotropic velocity structure. In the presence of an isotropic, low-velocity anomaly comparable to that imaged beneath the East Pacific Rise, there are only minor differences between the predicted signals of two- and three-dimensional (diapiric) flow. Tomographic modeling is used to determine if the synthetic data for a diapiric model (with a low-velocity isotropic anomaly) can be fit by two-dimensional anisotropy and three-dimensional velocity variations. The recovered isotropic anomalies are in good agreement with the synthetic model. However, if the diapir is large enough, artifacts are generated near the corners of the model and, locally, at the ridge axis, with slightly higher velocities. Our results indicate that tomographic analyses of existing travel time data from the East Pacific Rise cannot be used to rule out the presence of diapirs beneath an active spreading center if they are similar in scale to those mapped in Oman.

Components: 8217 words, 6 figures.

Keywords: Ridge; mantle; diapir; tomography; East Pacific Rise; Oman.

Index Terms: 3035 Marine Geology and Geophysics: Midocean ridge processes.

Received 1 August 2002; **Revised** 5 May 2003; **Accepted** 7 May 2003; **Published** 12 July 2003.

Jouselin, D., R. Dunn, D. R. Toomey, Modeling the seismic signature of structural data from the Oman Ophiolite: Can a mantle diapir be detected beneath the East Pacific Rise?, *Geochem. Geophys. Geosyst.*, 4(7), 8610, doi:10.1029/2002GC000418, 2003.

Theme: The Oman Ophiolite and Mid-Ocean Ridge Oman Process

Guest Editors: Peter Keleman, Chris MacLeod, and Susumu Umino



1. Introduction

[2] Two opposing models of mantle upwelling and melt transport have been proposed for the fast-spreading East Pacific Rise (EPR). In one model, as the newly formed lithosphere moves away from the spreading center, asthenospheric material ascends passively beneath the rise in a sheet-like two-dimensional flow pattern [e.g., *Lin and Phipps Morgan, 1992; Parmentier and Phipps Morgan, 1990*]. In this situation, there is no rise-parallel flow and mantle streamlines move upward or outward with respect to the rise, whereas mantle-derived melt converges toward and is distributed uniformly beneath the spreading axis [e.g., *Spiegelman and McKenzie, 1987*]. Alternatively, another model postulates that as the mantle ascends and melts, density instabilities trigger mantle diapirs that form buoyant flow beneath the ridge axis [e.g., *Nicolas and Violette, 1982; Whitehead et al., 1984; Rabinowicz et al., 1984, 1987; Crane, 1985; MacDonald et al., 1991; Su and Buck, 1993; Wang et al., 1996; Barth and Mutter, 1996*]. In this case, both mantle and melt flow lines converge toward the spreading axis in diapirs that are thought to be melt rich and thus conduits for magma transport.

[3] A remarkable assortment of diapiric models have been either conceptually hypothesized or numerically modeled and few of these models agree as to the scale of mantle diapirs. Notably, the smallest diapirs are the only ones constrained by observational evidence, which thus far comes from structural mapping of ophiolites that are thought to represent the remains of paleofast spreading ridges [*Nicolas and Violette, 1982; Ceuleneer et al., 1988; Nicolas and Boudier, 1995; Jousselein et al., 1998*]. In the case of structural data from ophiolites, the characteristic radius of the largest diapirs is generally small, about 3 km (defined by the region of inferred vertical flow), and such features have been mapped at intervals of a few tens of kilometers along the paleoridge axis; some are spaced as close as 10 km [*Boudier et al., 1997*]. Since this spacing is small relative to the length of a typical EPR segment (50–100 km), it is suggested that several diapirs would supply magma to a single segment of the ridge. Data from ophiolites, however, do not constrain the depth extent of

inferred diapirs, thus it is unknown if these features extend a few or many tens of kilometers into the mantle. A second class of models, derived from the analysis of EPR bathymetry and crustal structure [*Whitehead et al., 1984; Crane, 1985; MacDonald et al., 1991; Wang et al., 1996; Barth and Mutter, 1996*], proposes that a single large diameter diapir (>10 km) feeds an entire ridge segment. While these two models differ considerably in scale, both include a component of rise parallel flow in the mantle.

[4] The largest predicted mantle diapirs are inferred from two-dimensional numerical modeling [e.g., *Su and Buck, 1993; Blackman et al., 1996*]. In this case, a two-dimensional geometry is imposed by the modeling technique such that the third dimension, which includes the diapir spacing, is neglected. The models produce a buoyancy-driven flow field that extends from the base of the crust downward to depths of 60 to 100 km. Such models predict that melt is confined to a relatively narrow region of high concentration beneath the rise axis. In contrast, the seismic results of the MELT experiment predict that basaltic melt is present in the mantle beneath the EPR at 17°S over a surprisingly broad region several hundred kilometers across, and extending to depths of at least 200 km [*MELT Seismic Team, 1998; Forsyth et al., 1998; Toomey et al., 1998; Hammond and Toomey, 2003; Dunn and Forsyth, 2003*]. Furthermore, modeling of waveform data from the MELT experiment further indicates that if a melt-rich, low-velocity column – rooting at 60 km depth and greater than 5 km in width – was present in this region, it would be detected in the data [*Hung et al., 2000*]. Thus the MELT results do not support the existence of large mantle diapirs, but cannot be used to rule out the existence of diapirs similar to those inferred from ophiolites studies.

[5] Recent active-source, seismic tomography experiments along the EPR, which constrain upper mantle structure at a scale comparable to that of the fieldwork made in the Oman ophiolite, provide a new means of possibly detecting diapirs beneath the East Pacific Rise. The first analyses of this kind made along the EPR [*Dunn and Toomey,*

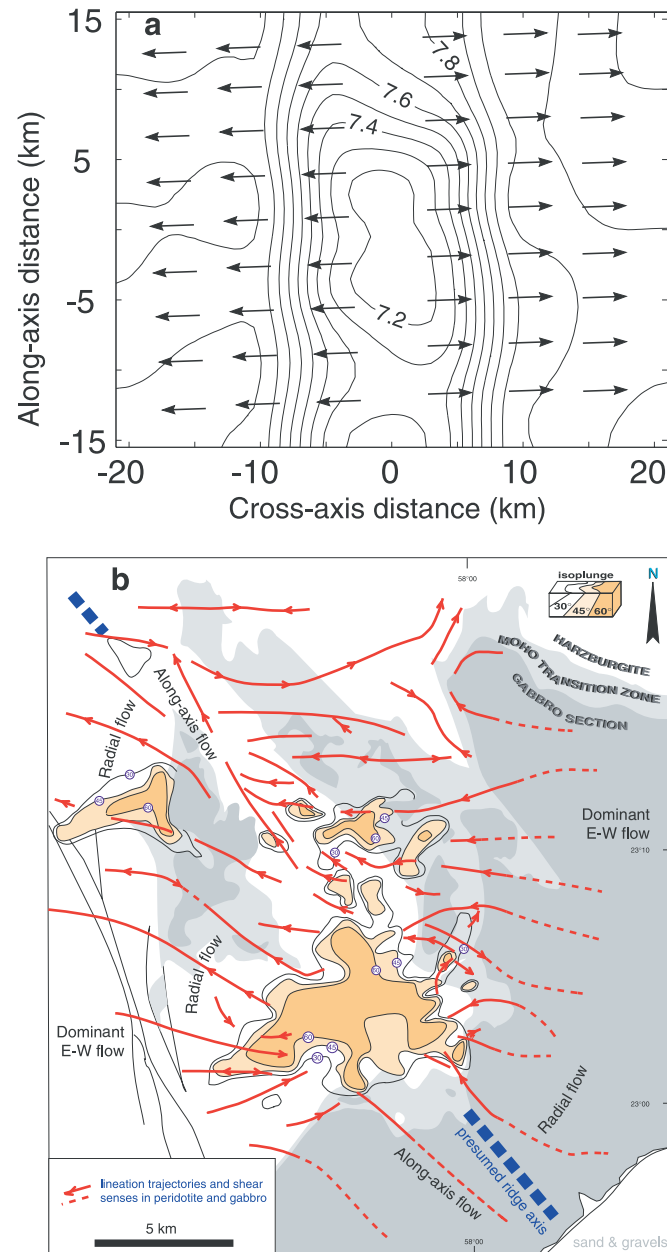


Figure 1. (a) Result of a tomographic inversion for the East Pacific Rise at $9^{\circ}30'N$, 1 to 4 km beneath the Moho (adapted from *Dunn and Toomey* [1997]). Contours of P wave velocity at intervals of 0.1 km/s; bars with arrows indicate the azimuth of anisotropy (crystallographic a -axis of olivine), under the assumption that the flow field is two-dimensional. (b) Lination map of the Maqсад diapir (adapted from *Jousselin et al.* [1998]). Note that the scale is approximately twice as large as that in Figure 1a.

1997; *Dunn et al.*, 2001] imaged mantle structures within 4 km of the Moho and within about 15 km of the rise axis (Figure 1). The results reveal the presence of an axially continuous low velocity zone beneath the Moho, which is modulated in amplitude, giving rise to localized volumes of more pronounced low-velocity anomalies. The

area of these local minima are approximately the size of the regions of radial flow that characterize the heads of ophiolite diapirs (~ 5 to 10 km) and they are spaced at irregular intervals of 10 to 20 km. Given the similarity in scale between the low-velocity, melt-rich regions detected beneath the EPR and the dimensions and spacing of



ophiolite diapirs, it is worth evaluating if the seismic data are consistent with diapiric flow.

[6] Since the alignment of the a-axes of olivine crystals during mantle flow produces seismic anisotropy [e.g., *Nicolas and Christensen, 1987*], seismic methods have the potential to map out variations in mantle flow fields. Here we present the results of forward and inverse modeling of seismic travel time data for anisotropic velocity models that replicate the structure of Oman ophiolite diapirs. Our goal is to determine whether seismic data collected by recent tomographic experiments along the EPR can detect or rule out the possibility of small-scale mantle diapirs similar to those inferred from the ophiolite studies. In a first step, the predicted seismic rays and P wave travel times of diapir models are compared to those of a synthetic model with three-dimensional velocity variations and a two-dimensional anisotropy field (uniform and perpendicular to the spreading axis), and to seismic data collected along the EPR. Although there are significant differences between the sets of travel times, there is no obvious characteristic that makes it easy to distinguish a pattern caused by diapiric flow. This raises the question: can data that contain anisotropy due to diapiric mantle flow be fit by a model with only two-dimensional anisotropy and three-dimensional velocity variations? In a second step we invert the synthetic travel times of the diapir models for isotropic velocity variations, using a starting model containing a fixed two-dimensional anisotropy pattern. Interpretations of the EPR data and considerations on how diapirs can be detected are discussed in reference to our results.

2. Oman Structural Data

[7] While the first mantle diapir mapped in an ophiolite was in the Philippines [*Nicolas and Violette, 1982*] the most complete data come from the Oman ophiolite, where it has been suggested that a paleoridge has been fossilized [*Boudier et al., 1997*]. Several studies have concluded that this paleoridge was fast spreading [e.g., *Boudier and Nicolas, 1985; MacLeod and Rothery, 1992*] in particular because of its continuous and magmat-

ically deformed gabbroic section. Uranium-lead dating has revealed age differences of the order of two million years for cross-strike distances exceeding 100 km, also consistent with a fast spreading rate [*Tilton et al., 1981*].

[8] In Oman, several diapirs have been mapped. One of them is interpreted as an off-axis diapir [*Jousselin and Nicolas, 2000*], whereas the others are thought to have underlain a paleoridge. This is well illustrated in the southern part of the ophiolite, where 4 diapirs have been mapped along a 150-km-long trend [*Boudier et al., 1997*]. The Oman diapirs are characterized by plunging lineations over an area less than 100 km² and an irregular pattern of radial flow extending 2 to 10 km away from a diapir's center [*Ceuleneer et al., 1988; Jousselin et al., 1998*]. The areas away from where diapirs are found are characterized by flat foliations with lineations that are consistently oriented at a high angle to the sheeted dike trend [*Boudier and Nicolas, 1985; Michibayachi et al., 2000*]. As the sheeted dike section is believed to correspond to the paleoridge orientation [*Helgasson and Zentilli, 1985; Auzende et al., 1989*], this suggests that away from diapirs, mantle flow is predominantly two-dimensional.

[9] Since the Maqsad diapir (Figure 1b) is particularly well mapped [*Jousselin et al., 1998*], we use it as an example for our seismic modeling. The structural data comprise 460 lineation measurements in a 16 × 22 km² area. Seventy-seven steeply plunging lineations (consistent with vertical flow lines) are found in a 30 km² area interpreted as the diapir's center, and about 30 more are dispersed in outliers north of the diapir. Nearby horizontal lineations are slightly diverging from the diapir, especially on the west side where they rotate from a direction parallel to the dikes trend (140°N) to an E-W direction. More regional mapping of the area records a large-scale E-W flow, which suggests that mantle flow was oblique to the 140°N paleoridge axis. The presence of a relatively thick (100 to 500 m) Moho transition zone (made of gabbroic sills interlayered in dunite, see *Boudier and Nicolas [1995]*), numerous chromite pods [*Ceuleneer and Nicolas, 1985*] and dike intrusions [*Jousselin et al., 1998*], along with geochemical



data [Godard *et al.*, 2000] indicate that mantle diapirs are regions of greater melt flux than the surroundings. Still, as the rocks have been compacted during cooling, it is not possible to determine what was the large scale melt fraction and distribution at the time the Oman paleoridge was active, except that a large amount of melt must have accumulated at the top of diapirs, thus forming the thick Moho transition zone. Even where it is the thickest, the Moho transition zone is still a small feature compared to seismic refraction wavelengths, and probably cannot influence tomographic images, but it may contribute to compliance results [Crawford *et al.*, 1999] and to seismic phases [Garmany, 1989] that are sensitive to the presence of melt sills even of meter scale.

3. EPR Seismic Data and Comparison With Simple Flow Models

[10] Two separate seismic tomography experiments have imaged the uppermost 4 km of the mantle below the EPR, one at $9^{\circ}30'N$ [Dunn and Toomey, 1997; Dunn *et al.*, 2000] and one at the $9^{\circ}03'N$ overlapping spreading center (OSC) [Dunn *et al.*, 2001]. The latter experiment is part of a larger data set collected between the Siqueiros ($10^{\circ}10'N$) and Clipperton ($8^{\circ}20'N$) fracture zones. Data from this experiment are being used to map mantle structure along and across a 230-km-long segment of the EPR. In both experiments, the seismic data were obtained by the undershooting technique, wherein sources and receivers populate lines located 10 to 20 km to either side of the rise (Figure 2). For this geometry, the first arrivals that travel beneath the axis of accretion are mantle-turning (Pn) phases. Pn rays enter the mantle at a lateral distance of about 5 km from a source or receiver, thus the region of the mantle sampled by data extends approximately 15 km to either side of the rise. The $9^{\circ}30'N$ experiment yielded 225 Pn travel time arrivals identified on 7 instruments (Figure 3a). The $9^{\circ}03'N$ experiment, which was specifically designed for imaging mantle structure, provided 2977 Pn arrivals from 1327 shots (Figure 3b); arrivals were identified on 15 stations, 9 of which recorded the shots on two different sensors. For the modeling presented below, we calculate synthetic

data for an experimental geometry that is comparable to that of the $9^{\circ}03'N$ experiment (Figure 2b). The delay time data from the undershooting experiments included evidence for upper mantle seismic anisotropy and thus were analyzed using a tomographic method that includes the effects of hexagonally anisotropic structure [Dunn and Toomey, 1997]. This form of anisotropy is observed in peridotite samples [e.g., Ben Ismail and Mainprice, 1998] and it is particularly useful for modeling azimuthal variations in seismic wave speed, which previous seismic studies have documented in Pn data from the Pacific Ocean [e.g., Raitt *et al.*, 1969]. Seismic anisotropy in this setting is attributed to the lattice preferred orientation of the a -axis of olivine crystals in the direction of mantle flow [e.g., Nicolas and Christensen, 1987]. To illustrate the signature of anisotropy in travel time data of Pn waves, we used the method of Dunn and Toomey [1997] to trace rays through anisotropic structures that do not contain isotropic variations in structure, such as the low-velocity zone beneath the rise. The isotropic mantle velocity is taken to be 7.8 km/s, and the magnitude of anisotropy is 6%, in agreement with the results of Dunn and Toomey [1997]. This leads to a maximum velocity of 8.03 km/s along the fast direction and a minimum of 7.57 km/s perpendicular to it.

[11] Results of these forward calculation are presented in Figure 3. For a two-dimensional model of anisotropy (Figures 3c and 3d), the resulting delay time signal (Figure 3e) is characterized by a $\cos(2\theta)$ pattern of delays, where θ is the angle between the propagation direction and the azimuth of the hexagonal symmetry axis. Minimum (maximum) delays correspond to rays propagating parallel (perpendicular) to the fast velocity axis. To first order, the Pn travel time data from the undershooting experiments (Figures 3a and 3b) also exhibit a $\cos(2\theta)$ pattern, thus the previously published tomographic images were obtained using a model that included a uniform, two-dimensional anisotropy field. In the actual data, most delays are positive because of the contributions of the low velocities beneath the rise. Inversion of the actual data thus results in tomographic images that feature an axially continuous region of anomalously low velocities

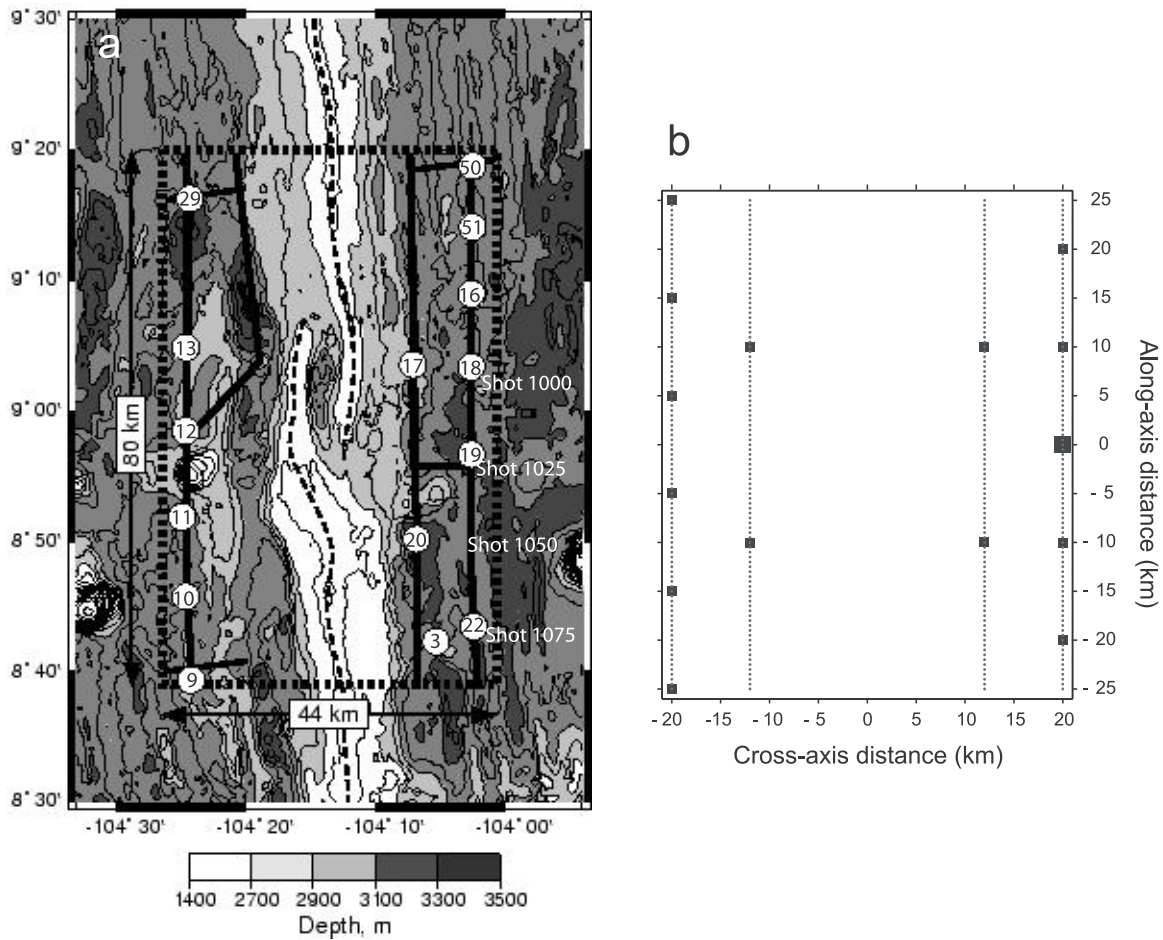


Figure 2. (a) Geometry of the undershoot seismic experiment from *Dunn et al.* [2001], receivers are circled numbers, shots occurred along the heavy black lines, shots 1000, 1025, 1050, 1075 are indicated for reference in Figure 5. Bathymetric contours every 100 m, grading from 1400 m (white) to 3500 m (dark). See *Dunn et al.* [2001] for more details. (b) Experimental design used for the synthetic modeling. Scale differs from Figure 2a. Dots indicate source positions; there are two lines of 101 shots on either side of the rise. Squares indicate the receiver locations; the largest square indicates the station for which synthetic data are shown in Figure 5.

with reductions varying from 4 to 12% relative to off-axis upper mantle velocities (e.g., Figure 1a). While these results can account for the large variations in the travel time delays departing from the $\cos(2\theta)$ pattern, they do not address the issue of whether some of the travel variations are due to an irregular anisotropy field that is characteristic of diapiric flow.

[12] The delay time signature of three- versus two-dimensional flow is significant; yet subtle when the radius of the head of the mantle diapir is less than 10 km. Figure 3g shows the predicted delay time for a perfectly symmetric mantle diapir (Figure 3f). As for the uniform flow model, the residuals by

azimuth also show, to first order, a $\cos(2\theta)$ signal; this is due to the background uniform flow in which the diapir is embedded. Superposed on this delay time pattern are anomalies of up to 100 ms, centered on the rise perpendicular direction. These anomalies are five times greater than the typical uncertainty in an actual measurement (~ 20 ms), suggesting they can be considered as seismically detectable. Still, note that for both models the delay time signature of anisotropy has an amplitude (difference between the maximum and the minimum delay) of about 200 ms, which is less than half of that observed in the actual experiments when similar azimuthal coverage is compared (Figure 3b). This result is consistent with isotropic

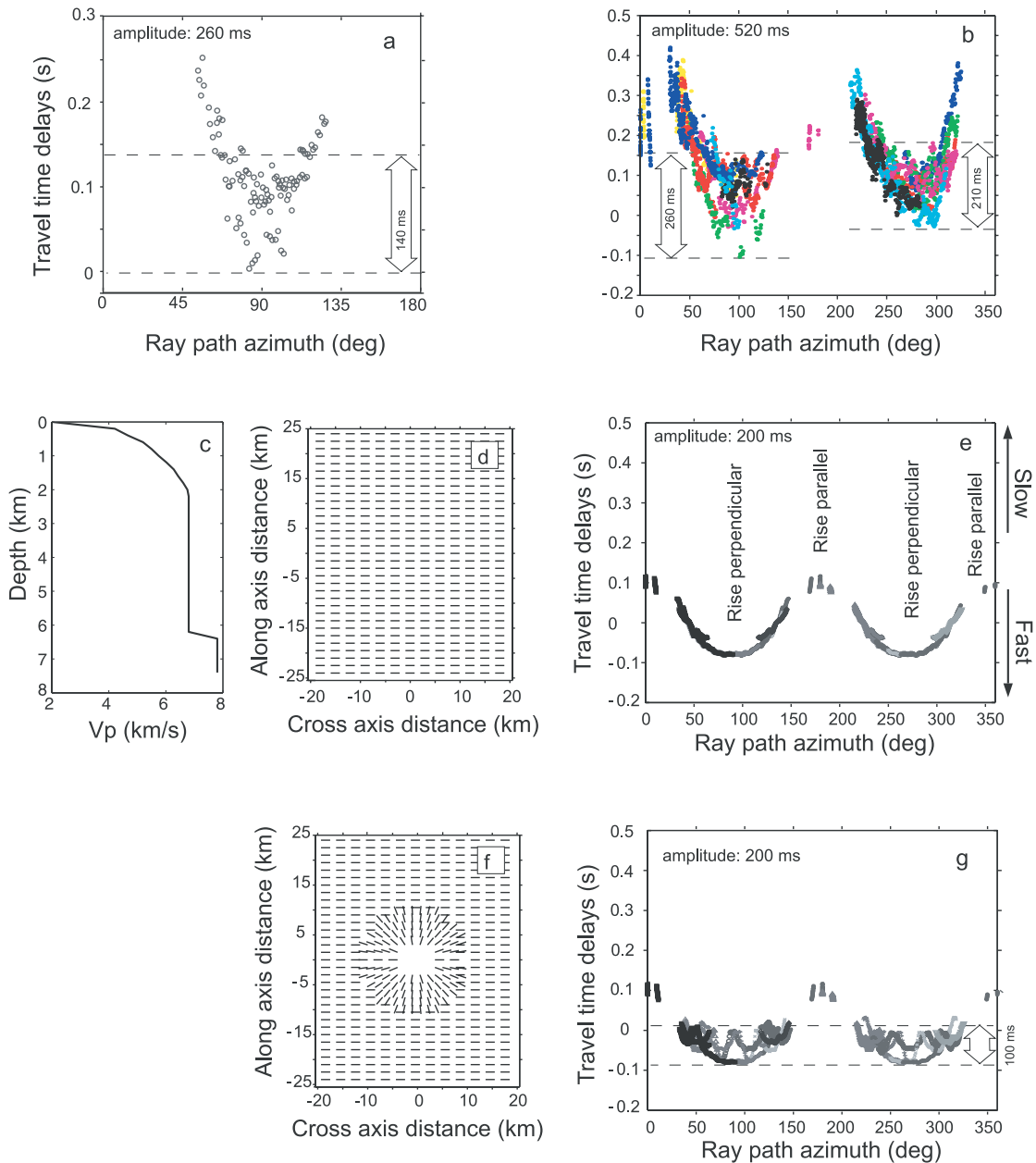


Figure 3. Travel time delays from (a) the $9^{\circ}30'N$ experiment [Dunn and Toomey, 1997] and (b) the $9^{\circ}03'N$ OSC experiment [Dunn et al., 2001]. Delays are the difference between actual travel times and the travel times calculated for a one-dimensional (depth varying), isotropic reference model as shown in Figure 3c. Each symbol corresponds to one delay calculated for a shot-receiver pair. In Figure 3b a different color is used for each station's delays. Delay uncertainties are 10 to 30 ms and are plotted by ray azimuth; angles of 90° and 270° are rise perpendicular; data at angles $<180^{\circ}$ ($>180^{\circ}$) are for stations on the east (west) side of the rise recording shots on the opposite rise flank. Note that for Figure 3a the relative amplitude as compared to Figure 3b is apparently lower because of limited azimuthal coverage. Variations of delays for rays within 40° of the rise perpendicular direction are indicated within white double arrows. (c) The velocity profile used for the following models and delay calculations in this study are shown. (d, e) A two-dimensional flow model (bars indicate the azimuth of the crystallographic a -axis of olivine; the seismic anisotropy is 6% and is present only below the Moho, i.e., at depth of 6.4 km and more) and the associated synthetic travel time delays is shown. Rays that cross the rise at 90° arrive earlier (less delay) than those that travel obliquely to the rise. (f, g) A perfectly radial flow model and the associated synthetic travel time residuals is shown. The dimensions of the diapir in Figure 3f are approximately that of the diapirs mapped in Oman. To show the relative importance of the anisotropy field to delay time data, the models do not include any isotropic heterogeneity.



heterogeneity giving rise to much of the observed delay time anomalies; hence it is possible that delays due to irregularities in the anisotropy field are interpreted as small isotropic velocity anomalies during the inversion process.

[13] Calculations presented below differ in several ways from those presented by *Dunn et al.* [2000]. The size of some of the mantle diapirs tested by *Dunn et al.* [2000] were generally larger than structures mapped in Oman and thus gave rise to delay time patterns that differed more dramatically in comparison with uniform flow [*Dunn et al.*, 2000, Figure 7e]. Also, our calculations here combine the effects of flow induced seismic anisotropy with isotropic low-velocity anomalies typical of the EPR; this considerably alters the rough $\cos(2\theta)$ signal due to the anisotropy models. Finally, we present for the first time the results of inverting synthetic data from diapiric models.

4. Seismic Modeling of OMAN Diapirs

[14] We built diapir models with mantle anisotropy azimuths and dips based on the lineation map of the Maqsad area. As the Maqsad diapir is not symmetric and variations can be found from one diapir to another, we envisaged different cases combining the possible ranges for the relative amounts of radial versus vertical flow. Three models are presented in this study (Figure 4), they differ only in the orientation of the mantle anisotropy that we impose in the mantle section. One model is derived from the Maqsad map, with radial flow extending more on the west flank than on the east flank (Figure 4e). Another one reduces the amount of radial flow on the west side to be the same as that found on the east side (Figure 4c). This results in a smaller head for the diapir, more like the one mapped near Nakhl [*Nicolas and Boudier*, 1995; *Jousselin*, 1998]. Conversely, in the third diapir model, the amount of radial flow on the east of the Maqsad-like model, is increased to match the amount found to the west (Figure 4g). This results in a larger diapir, similar to the one in the Rustaq area [*Nicolas and Boudier*, 1995]. In all models the mantle background anisotropy is taken to be two-dimensional so that the fast axis of

propagation (the crystallographic a -axis of olivine) is oriented parallel to the spreading direction 10 km away from the ridge axis. The magnitude of anisotropy is 6%.

[15] As we do not know the melt content of an Oman-like diapir, we cannot use ophiolite data to infer the associated isotropic velocity anomaly. Given that the area of the mantle velocity anomalies detected beneath the EPR at $9^{\circ}30'N$ and $9^{\circ}03'N$ are comparable to dimensions of the top of an Oman diapir, we use an isotropic velocity model derived from tomographic imaging (Figure 4a); away from the regions with anomalies, the average mantle velocity is 7.8 km/s. The complete model is parameterized as follows: the top of the model begins at the seafloor, which is taken to be horizontal and overlain by 2500 m of water. The crust is 6.2 km thick, with a one-dimensional velocity structure taken from averaging the off-axis crustal velocities reported in *Dunn et al.* [2001] and is typical of Pacific ocean crustal velocities (Figure 3c). The model volume is $41 \times 51 \times 10 \text{ km}^3$ with the longest and shortest dimensions being rise parallel and vertical, respectively. For ray tracing, the grid spacing is 250 m horizontally and 200 m vertically; this is identical to that used in the actual EPR studies. To approximate the design of the most recent undershoot experiment (Figure 2a), we calculate travel times between 15 receivers spaced every 10 km and 404 shots spaced every 500 m (Figure 2b), yielding a total of $\sim 2500 Pn$ arrivals. This includes 2 inner lines located 12 km from the ridge axis along which there are four stations. This modeling geometry has a more uniform ray coverage than the actual experiments, so that we can capture any specific signal that would be caused by diapiric flow (i.e., variations in anisotropy).

5. Synthetic Travel Times of Diapir Models

[16] The results of the forward modeling calculations are presented in Figure 4. Travel time delays with respect to the reference model are plotted by azimuth of the ray path. The results for diapir models (Figures 4d, 4f, and 4h) can be compared

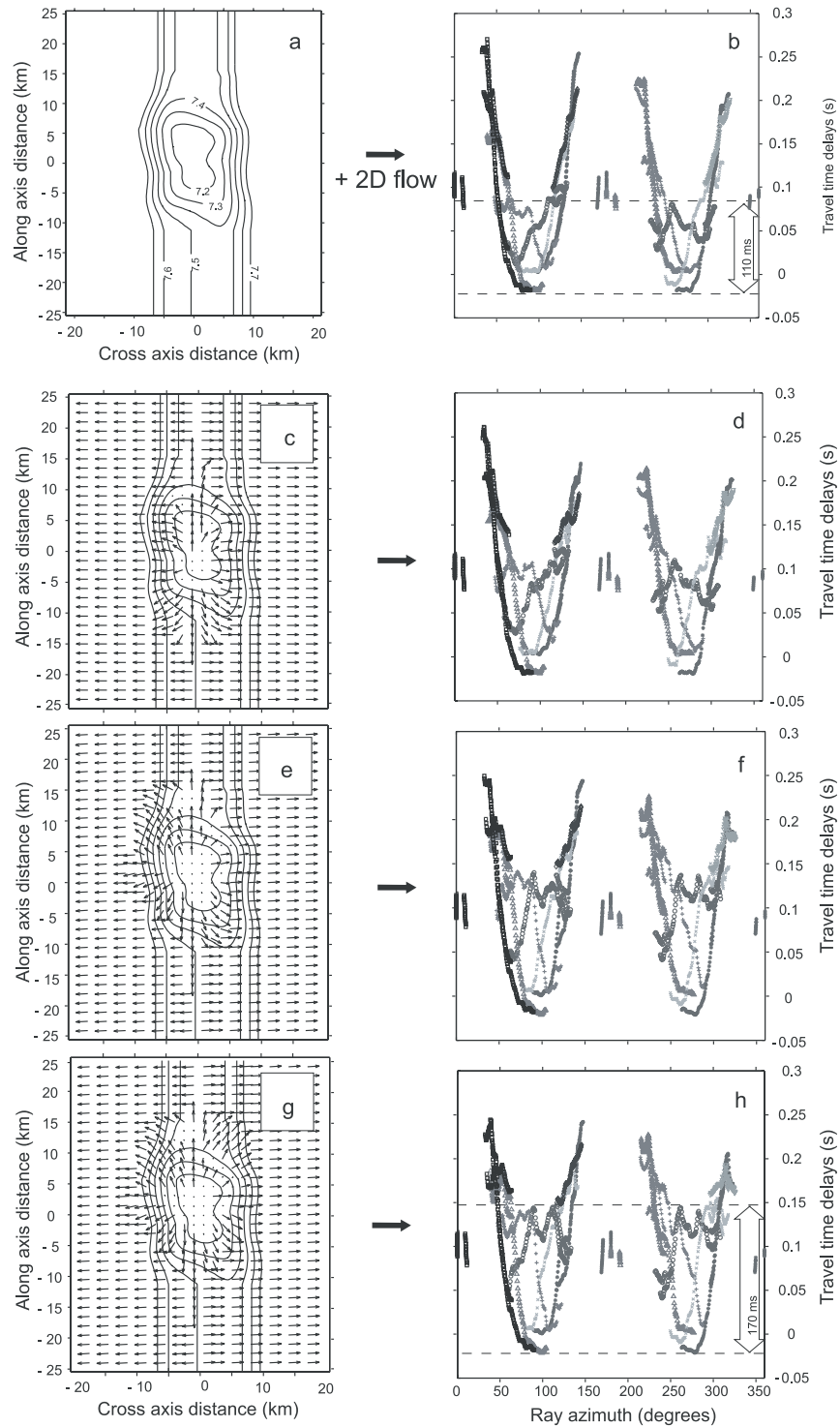


Figure 4. Results of the forward modeling calculations for several different geometries of seismic anisotropy that include the same model of isotropic heterogeneity. (a) Contour map of the isotropic velocity anomaly superposed on two-dimensional and diapirs flow models (map at 6.4 km depth and more, contour interval is 0.1 km/s, see Figure 3c for shallower velocities and Figure 3d for the two-dimensional flow field). (b) Synthetic residual data for the two-dimensional flow model. (c, e, g) Anisotropy fields for three different diapirs are shown; see text for discussion. (d, f, h) The associated pattern of residuals are shown. Symbol types and shapes indicate different receivers; Variation of delays for rays within 40° of the rise perpendicular direction are indicated with double arrows in Figures 4b and 4h for comparison with Figure 3.



to that of a two-dimensional-flow model with the same isotropic velocity anomaly (Figure 4b). Differences between the models are not as striking as they are between a two-dimensional flow model and a “perfect diapir” with no isotropic velocity anomaly (Figures 3e and 3g). Viewed as a whole, delay time patterns exhibit an irregular U-shaped trend with comparable amplitudes (300 ms for the two-dimensional model, 270 to 300 ms for diapir models). For rays with an azimuth near 90° and 270° (rays perpendicular to the rise) diapir models have a larger variation of delays (up to 170 ms between the earliest and the latest arrivals) than for the two-dimensional-flow model (110ms).

[17] A more subtle difference, that is barely present for the smallest diapir, is the presence of a few more inflection points in the pattern of residuals plotted by azimuth. These inflection points are associated with stations that are closest to the diapir. Consider in detail the arrivals recorded at the central station on the east side of the model (Figure 5). In the two-dimensional flow model, delays have a simple U-shaped trend, either steadily decreasing or increasing, with only one inflection point at an azimuth within 20° of the rise-perpendicular direction. In contrast, diapiric flow results in several inflection points that are located at angles of up to 35° from the rise perpendicular direction. In the case of a diapir, an inflection point sometimes marks the passage from increasing to decreasing delays with increasing angles, thus forming a rough M-shaped anomaly. In the case of two-dimensional flow, an inflection point is always a component of a U-shaped anomaly. Figure 4 also shows that where a rough M-shaped anomaly is observed, some other arrivals with the same ray azimuth appear much earlier. These differences are still detectable when random noise is added to the synthetic data (with a standard deviation similar to noise levels for real data) (Figures 5c and 5d). Among all the models that were tested - including some not shown here - the smaller diapir models (Figure 4c) give rise to delays that are the most similar to that of the two-dimensional flow model (Figure 4b), whereas the larger diapirs (Figure 4h) result in delays that are

the most different from those of two-dimensional flow.

[18] Data from the actual experiments have delay time anomalies that are comparable in amplitude and trend to that of our synthetic models. A comparison of Figure 4 with Figures 3a and 3b shows that the amplitude of a delay time anomaly is about ~300 ms for the same azimuthal coverage. For ray azimuths approximately perpendicular to the rise, the actual data from the EPR (Figures 3a and 3b) vary by about 210 ms, which is more than our synthetic data (Figure 4). Also, most of the EPR data (but not for all stations) have trends that do not depart significantly from a rough U-shaped pattern. In Figure 5e, we have isolated arrivals recorded at three selected stations from the 9°03'N OSC experiment [Dunn *et al.*, 2001]. Station arrivals are plotted in gray. Except for a small step at ~80° azimuth, it recorded a simple U trend, with shots across the rise (90–100° azimuth, around shot 1046) arriving earlier than shots at oblique angle. However, unlike in the modeling, there is no continuous coverage of shots at angles from 50 to 150°. This is well illustrated by this particular station where no arrival was identified at angles greater than 130° (shots north of shot 1036 on Figure 2), thus making a complete comparison with the modeling difficult. Such interruption in coverage sometimes corresponds to rays that cross attenuating low-velocity regions, where *P_n* phases become difficult to pick (Figure 5f). The two other examples have better azimuthal coverage, with station 9 (black) recording shots 1024 to 1092, and station 11 (open symbols) recording shots 934 to 1092. Arrivals plotted as open circles have three easily identified inflection points (at azimuths of ~110°, 135°, 150°), and arrivals in black exhibit inflection points that are perhaps less easily identified (near azimuths of 75°, 100°, 120° and 145°). Interestingly, in those two cases, inflection points at ~150° are more than 35° to the rise direction. Also, arrivals shown in black may exhibit multiple inflection points at azimuths that are associated with earlier arrivals at other stations, as predicted by diapir modeling. The same type of analysis can be made for the first undershoot experiment [Dunn and Toomey, 1997], but as there are 10 times fewer

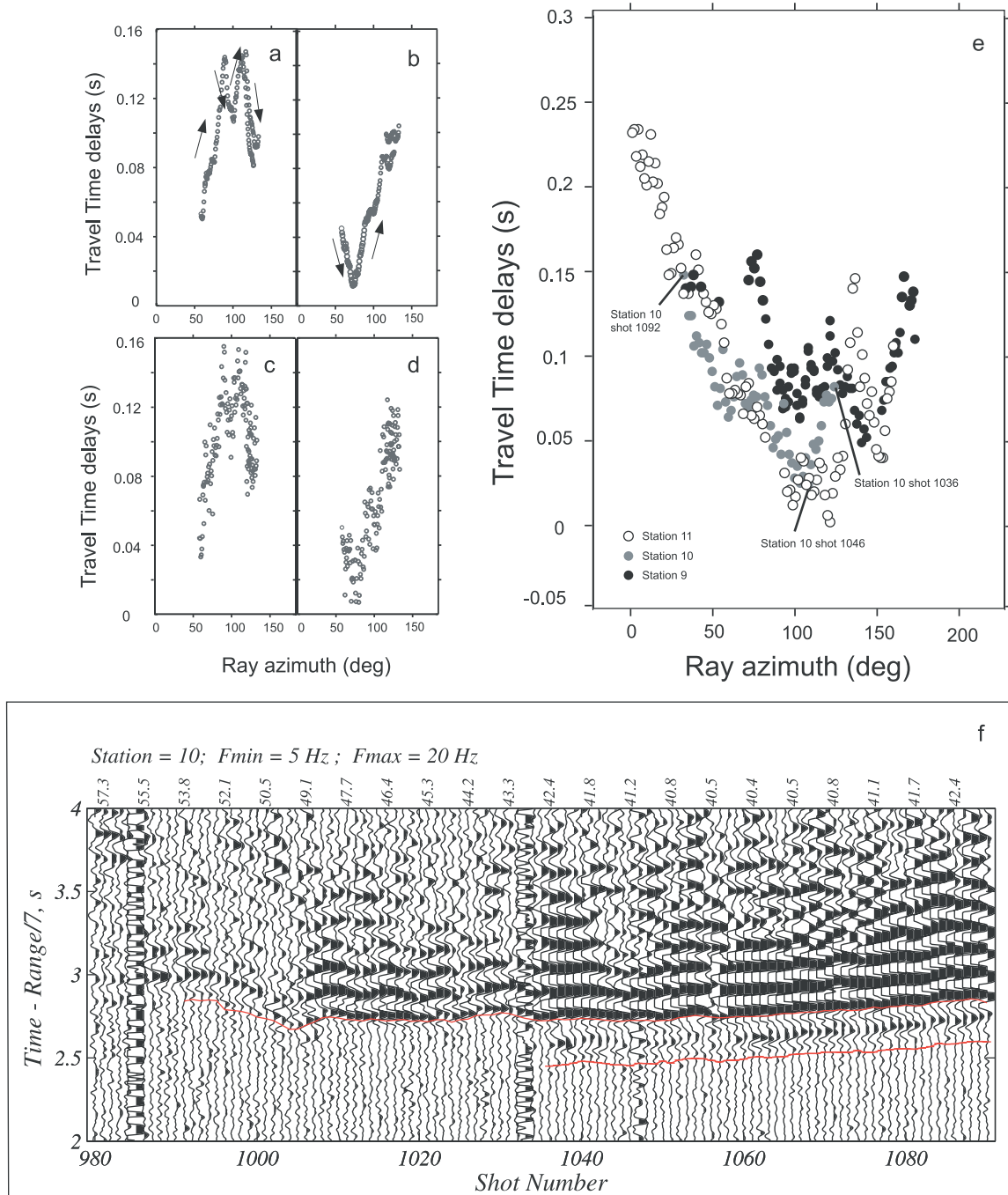


Figure 5. Plots of synthetic and actual delay time residuals; latter are from the $9^{\circ}03'N$ experiment. All synthetic data are shown for the central station on the east side of the ridge (indicated by larger square in Figure 3). (a) Synthetic residuals for the diapir model of Figure 4g. (b) Synthetic data for a two-dimensional-flow model (Figure 4a). (c, d) The same as in Figures 5a and 5b, respectively, except that random, normally distributed noise has been added to the synthetic data (variance of 0.015 s); (e) a subset of data recorded by three stations from the $9^{\circ}03'N$ OSC experiment (different symbols are used for each station; the entire data set is shown on Figure 2b; the 3 stations being on the west side of the ridge, and considering the convention used in Figures 3 and 4, P_n azimuths should be between 180 and 360° , but 180° have been subtracted to make the x axis more readable). Note that the scale is the same as in Figures 5a–5d. Arrows in Figures 5a and 5b are shown to indicate trends and differences in the position of inflection points. (f) Record section of receiver 10 for shots whose delays are represented in Figure 5e. Two red lines indicate where P_n and P_mP have been picked. Station position and approximate shots position can be seen in Figure 2a.



data in that experiment than in our modeling it lacks sufficient azimuthal coverage, making direct comparisons less meaningful. Another difficulty in the analysis of real data is the effect of the crustal structure, which is three dimensional, unlike in the modeling. This effect can be removed if the reference model used to calculate Pn delays accurately reflects the crustal structure (which is constrained by Pg and PmP data); if it is not perfectly removed, it can produce inflection points on top of those due to the mantle structure. In summary, a comparison of actual seismic data with the delay time signature of diapiric models suggests that both data have comparable delay time trends. Since the signature of diapiric flow tends to be subtle, it is as yet difficult to conclude that the actual seismic data either require the presence of diapiric flow, or altogether rule out this possibility. Instead, from forward modeling, it appears as though the actual data are equivocal with regards to the existence of diapirs comparable to those mapped in Oman.

6. Results of Tomographic Inversions

[19] To provide a quantitative analysis of the effects of anisotropy patterns on the interpretation of mantle seismic structure, we tomographically inverted the synthetic travel time data for the two-dimensional and diapiric flow models shown in Figure 4 following the procedure of *Dunn et al.* [2000]. The starting crustal velocity model was the same as that of the forward modeling, the mantle velocity was taken as 7.8 km/s, with a uniform anisotropy of 6% (i.e., the starting model correspond to the model shown in Figures 3c and 3d). This procedure tests the degree to which the assumption of two-dimensional flow (uniform anisotropy), used by *Dunn and Toomey* [1997] and *Dunn et al.* [2001], biases the tomographic reconstruction of a known isotropic velocity anomaly. Figure 6a shows the results of tomographic inversion of data derived from the two-dimensional flow model of Figure 4a. This result demonstrates that the available ray set can accurately reconstruct the known isotropic velocity anomaly. Figures 6b–6e show the results of inverting the synthetic data calculated for the different mantle diapir models under the assumption of two-dimensional flow. For

each of the models shown in Figure 4, we were able to obtain tomographic results that provided a reasonable fit to the data ($\chi^2 = 1$ to 1.2). For the smaller or Maqsad-like diapirs (Figures 6b and 6c, respectively), we obtained acceptable results for a single set of smoothing parameters (these control the smoothness of the velocity solution). However, in the case of the larger diapir model (Figure 4g), the same smoothing parameters resulted in a model (Figure 6d) with a significantly larger and unacceptable χ^2 value of 1.6. For this model we had to substantially decrease the spatial smoothing to obtain a statistically acceptable fit to the data ($\chi^2 = 1.0$). The resulting tomographic image of isotropic heterogeneity (Figure 6e) includes several artifacts whose dimensions approach the dimensions of true velocity features that are resolvable with the experiment geometry (see the resolution tests presented by *Dunn et al.* [2001]). In other words, if such features were present in the inversion of actual data, one might conclude that they were well resolved features of the velocity field.

[20] Further inspection of Figure 6 shows that the tomographic inversions were able to reconstruct the overall mantle velocity anomaly except in the case of the largest mantle diapir. For example, the reconstructed anomalies in Figures 6a–6c are all comparable in terms of their location, shape and amplitude of the known anomalous structure. In contrast, the results obtained for the largest diapir include artifacts that are large and geologically implausible. In detail, regions where radial flow extends further from the rise axis induce the formation of short wavelength cross-axis velocity variations. This is most visible just south of the center of the model (rise-perpendicular coordinate -10 km of Figure 6e) where a velocity of 7.4 km/s is found beneath the rise (cross-axis coordinate 0 km) and juxtaposed with off-axis regions of slower velocity (7.3 km/s at cross-axis coordinates of ± 5 km). This arrangement of velocity anomalies does not seem geologically plausible, as we would expect the lowest velocities to be centered beneath the rise, instead of bounding a region of faster, sub-axial velocity. To a much lesser degree, this pattern is also observed to the south of the model for the Maqsad-like diapir (Figure 6c). Another artifact

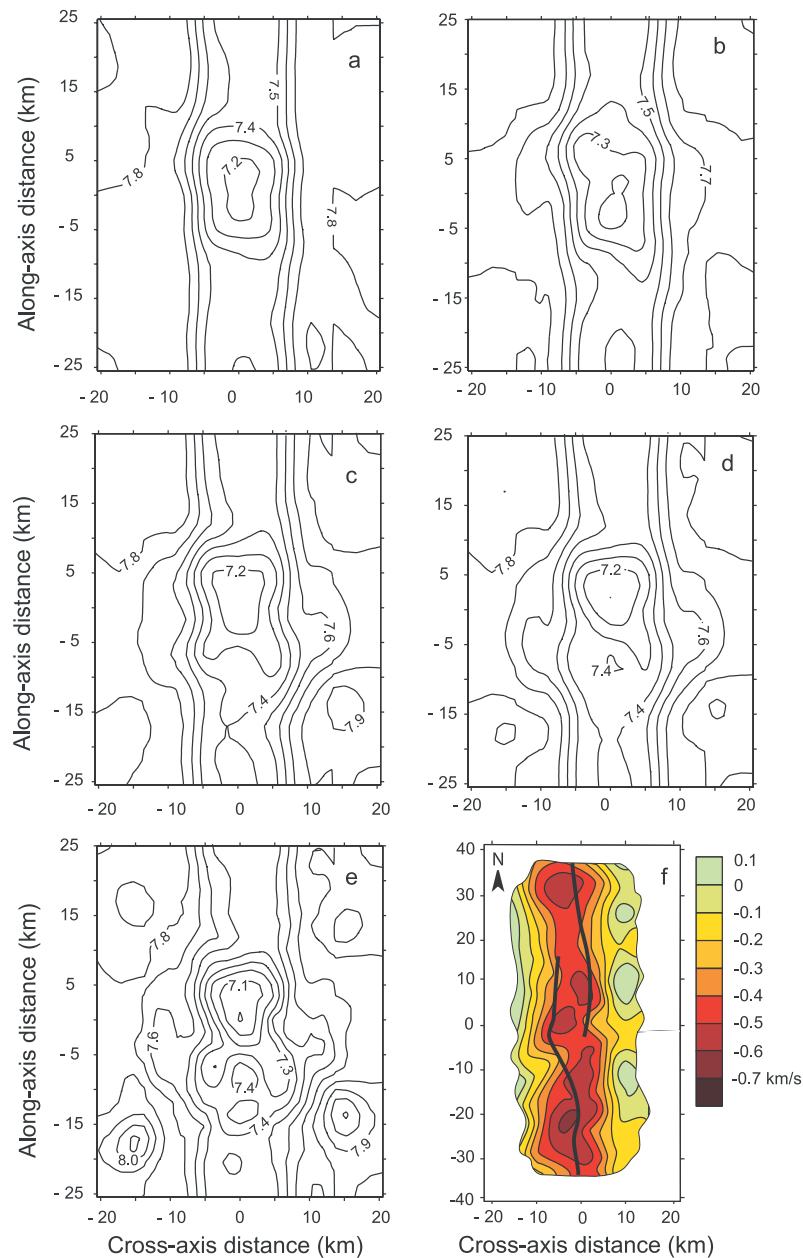


Figure 6. Results of tomographic inversions of synthetic data for models shown in Figure 4. Horizontal slices at 6.4 km depth, except in Figure 6f. In all cases, the models contain a two-dimensional field of anisotropy not shown here for clarity; contour interval is 0.1 km/s. Prior to inversion of diapir models, random noise (variance of 0.015 s) was added to the synthetic data. (a) Result of the inversion for data derived from the model shown in Figure 4a. (b) Result of inversion for a small diapir ($\chi^2 = 1$), shown in Figure 4c. (c) Result of inversion for a Maqsad-like diapir ($\chi^2 = 1.2$), shown in Figure 4e. (d) Result of inversion for the larger diapir of Figure 4g with the same smoothing as in Figure 6a and 6b ($\chi^2 = 1.6$). (e) Result of inversion for the larger diapir, with less spatial smoothing ($\chi^2 = 1$); note the presence of significant artefacts both beneath the rise and near the corners of the model. (f) Result of the $9^{\circ}03'N$ experiment, horizontal slice at 7 km depth; contours indicate velocity perturbations with respect 7.8 km/s; the black lines indicate the position of the ridge axes, only the region with a good population of P_n rays is shown, see *Dunn et al.* [2001] for details.



characteristic of inversions of data for the largest diapir model is the presence of anomalously high velocities (>7.8 km/s) near the corners of our models (Figure 6e). Figure 6f shows results of tomographic imaging by *Dunn et al.* [2001]. It presents three high velocity zones on the east side of the rise and a slightly contorted central low velocity zone that may be due to anisotropic variations. However, considering the complex geological setting (an overlapping spreading center with an inflated ridge segment at the south, see Figure 2a and *Dunn et al.* [2001] for details) irregularities in the low velocity zone might be expected and such features are not discriminative regarding the diapir hypothesis. Lastly, Figure 6 shows that as the size of the diapir increases, the reconstructed low velocity anomaly beneath the rise increases in magnitude. This trade-off results from an increase in the cross-sectional area with sub-vertical flow lines; when the a -axis is vertical, the slow propagation direction is horizontal and in the direction of Pn propagation.

[21] Results of our forward and inverse tomographic modeling show the difficulty of isolating the effects of anisotropy on travel time data in an area with irregular velocity variations of up to 1 km/s (12% variation). We show that diapiric flow and associated anisotropy should have a clear influence on seismic data if diapirs are sufficiently large (i.e., radial flow is present more than 10 km away from the diapir center). On the other hand, if travel time data are well fit by uniform anisotropy representative of two-dimensional flow, we have shown that (1) this does not exclude the hypothesis that a diapir may be present, (2) the low velocity zone is relatively well resolved in spite of the neglect of secondary variations in anisotropy structure. A problem with identifying radial anisotropy structure is the spacing of stations relative to the size of the diapir structure. In Figure 4c, only the southern part of the diapir (lower part of the figure) shows anisotropy oblique to the x axis over an area larger than 5 km. Thus only a couple of stations can detect this structure. This problem is compounded in real experiments because stations do not always record complete lines of shots as some shot energy is absorbed in low velocity

areas. Deploying additional stations across the rise, including near the rise, and perhaps more densely spaced overall, would greatly improve the sampling of the anisotropy.

7. Conclusions

[22] We have calculated synthetic travel times of melt-rich mantle diapir models with anisotropy derived from the Maqсад diapir (Oman ophiolite) structural maps and three-dimensional isotropic velocity variations taken from EPR seismic experiments. The results have been compared with that of a two-dimensional flow model containing the same three-dimensional isotropic velocity variations, and with EPR seismic data. We find that a small - but geologically reasonable - diapir would not yield easily detectable effects in travel time data. Larger diapirs may give rise to detectable effects, provided there is enough high quality data. On the basis of our forward and inverse modeling, we can now anticipate how radial flow may be expressed in our data and in tomographic images. First, for stations recording arrivals that are nearest to an actual diapir, the trend in residuals plotted by azimuth of the ray will include a succession of inflection points, particularly for rays near the rise perpendicular direction. This is true even for small diapirs, hence, if this is not seen in well sampled data - which is not the case - one may exclude the diapir hypothesis. Second, if diapirs are large, tomographic images obtained under the assumption of two-dimensional flow may include a succession of low and high velocities *across* the ridge, departing from the usual along axis variations. We conclude that if a mantle diapir exists beneath the EPR, it will be difficult, but not impossible, to detect its presence using current seismic techniques. This is especially true if the diapir is embedded in a background of two-dimensional flow, as is the case for diapirs mapped in the Oman ophiolite. Thus the three-dimensional melt distributions found to date at the EPR [*Dunn and Toomey, 1997; Dunn et al., 2001*] may be attributed to variations in the melt content along the rise, superposed with either a two-dimensional or three-dimensional flow field, particularly if the latter is associated with a small-scale diapir. We note that if diapirs of moderate size are



indeed present beneath the EPR, tomographic maps of seismic velocity heterogeneity are not significantly biased by the assumption that mantle flow is two-dimensional. Assuming that the mantle low velocity zones are relatively stable in time, the good accuracy produced by current data could allow to plan different types of experiments that would focus on one specific low velocity zone.

Acknowledgments

[23] This research was supported by a RIDGE postdoctoral fellowship, OCE- 9810860 and by NSF grants OCE-9633264, OCE-0118597 and OCE-0224903. We would like to thank two anonymous reviewers for their comments on the manuscript.

References

- Auzende, J. M., D. Bideau, E. Bonatti, M. Cannat, J. Honnorez, J. Malavieille, V. Mamaloukas-Frangoulis, and C. Mevel, Direct observation of a section through slow-spreading oceanic crust, *Nature*, *337*, 726–729, 1989.
- Barth, G. A., and J. C. Mutter, Variability in oceanic crustal thickness and structure: Multichannel seismic reflection results from the northern East Pacific Rise, *J. Geophys. Res.*, *101*, 17,951–17,975, 1996.
- Ben Ismail, W., and D. Mainprice, An olivine fabric database: An overview of upper mantle fabrics and seismic anisotropy, *Tectonophysics*, *296*, 145–158, 1998.
- Blackman, K. D., J. M. Kendall, P. R. Dawson, H. R. Wenk, D. Boyce, and J. Phipps Morgan, Teleseismic imaging of subaxial flow at mid-ocean ridges: Traveltime effects of anisotropic mineral texture in the mantle, *Geophys. J. Int.*, *127*, 415–426, 1996.
- Boudier, F., and A. Nicolas, Harzburgite and lherzolite subtypes in ophiolitic and oceanic environments, *Earth Planet. Sci. Lett.*, *76*, 84–92, 1985.
- Boudier, F., and A. Nicolas, Nature of the Moho transition zone in the Oman ophiolite, *J. Petrol.*, *36*, 777–796, 1995.
- Boudier, F., A. Nicolas, B. Ildefonse, and D. Joussetin, EPR microplates, as a model for the Oman ophiolite, *Terra Nova*, *9*, 79–82, 1997.
- Ceuleneer, G., and A. Nicolas, Structures in podiform chromite from the Maqsd district (Sumail ophiolite, Oman), *Miner. Deposita*, *20*, 177–185, 1985.
- Ceuleneer, G., A. Nicolas, and F. Boudier, Mantle flow patterns at an oceanic spreading centre: The Oman peridotites record, *Tectonophysics*, *151*, 1–26, 1988.
- Crane, K., The spacing of rift axis highs: Dependence upon diapiric processes in the underlying asthenosphere?, *Earth Planet. Sci. Lett.*, *72*, 405–414, 1985.
- Crawford, W. C., S. C. Webb, and J. A. Hildebrand, Constraints on melt in the lower crust and Moho at the East Pacific rise, 9 degrees 48'N, using seafloor compliance measurements, *J. Geophys. Res.*, *104*, 2923–2939, 1999.
- Dunn, R. A., and D. W. Forsyth, Imaging the transition between the region of mantle upwelling and the crustal magma chamber with short-period Love wave propagation along the southern East Pacific Rise, *J. Geophys. Res.*, in press, 2003.
- Dunn, R. A., and D. R. Toomey, Seismological evidence for three-dimensional melt migration beneath the East-Pacific Rise, *Nature*, *388*, 259–262, 1997.
- Dunn, A. R., D. R. Toomey, and S. C. Solomon, Three-dimensional seismic structure and physical properties of the crust and shallow mantle beneath the East Pacific Rise at 9°N30, *J. Geophys. Res.*, *105*, 23,537–23,555, 2000.
- Dunn, R. A., D. R. Toomey, R. S. Detrick, and W. S. D. Wilcock, Continuous mantle melt supply beneath an overlapping spreading center on the East Pacific Rise, *Science*, *291*, 1955–1958, 2001.
- Forsyth, D. W., S. C. Webb, L. M. Dorman, and Y. Shen, Phase velocities of Rayleigh waves in the MELT experiment on the East Pacific Rise, *Science*, *280*, 1235–1238, 1998.
- Garmann, J., Accumulation of melt at the base of young oceanic crust, *Nature*, *340*, 628–632, 1989.
- Godard, M., D. Joussetin, and J. L. Bodinier, Relationships between geochemistry and structure beneath a palaeo-spreading centre: A study of the mantle section in the Oman ophiolite, *Earth Planet. Sci. Lett.*, *180*, 133–148, 2000.
- Hammond, W. C., and D. R. Toomey, Seismic anisotropy and heterogeneity beneath the MELT region of the East Pacific Rise from analysis of P and S body waves, *J. Geophys. Res.*, *108*(B4), 2176, doi:10.1029/2002JB001789, 2003.
- Helgason, J., and M. Zentilli, Field characteristics of laterally emplaced dikes: Anatomy of an exhumed Miocene dike swarm in Reydarfjörður, eastern Iceland, *Tectonophysics*, *115*, 247–274, 1985.
- Hung, S. H., D. W. Forsyth, and D. R. Toomey, Can a narrow, melt-rich, low-velocity zone of mantle upwelling be hidden beneath the East Pacific Rise? Limits from waveform modeling and the MELT Experiment, *J. Geophys. Res.*, *105*, 7945–7960, 2000.
- Joussetin, D., Structure détaillée et propriétés sismiques des diapirs de manteau dans l'ophiolite d'Oman, *Mem. Geosci. Montpellier*, *10*, 215, 1998.
- Joussetin, D., and A. Nicolas, Oceanic ridge off-axis deep structure in the Mansah region (Sumail massif, Oman ophiolite), *Mar. Geophys. Res.*, *21*, 243–257, 2000.
- Joussetin, D., A. Nicolas, and F. Boudier, Detailed mapping of a paleo-spreading center in the Oman ophiolite, *J. Geophys. Res.*, *103*, 18,153–18,170, 1998.
- Lin, J., and J. Phipps Morgan, The spreading rate dependence of three-dimensional mid-ocean ridge gravity structure, *Geophys. Res. Lett.*, *19*, 13–16, 1992.
- MacDonald, K. C., D. S. Scheirer, and S. M. Carbotte, Mid-ocean ridges: Discontinuities, segments and giant cracks, *Science*, *253*, 986–994, 1991.
- MacLeod, C. J., and D. A. Rothery, Ridge axial segmentation in the Oman ophiolite: Evidence from along-strike variations in the sheeted dike complex, in *Ophiolites and Their Modern Oceanic Analogues*, edited by L. M. Parson, B. J. Murton, and P. Browning, *Geol. Soc. Spec. Publ. London*, *60*, 39–63, 1992.



- MELT Seismic Team, Imaging the deep seismic structure beneath a mid-ocean ridge: The MELT experiment, *Science*, *280*, 1215–1218, 1998.
- Michibayashi, K., L. Gerbert-Gaillard, and A. Nicolas, Shear sense inversion in the Hilti mantle section (Oman ophiolite) and active mantle uprise, *Mar. Geophys. Res.*, *21*, 259–268, 2000.
- Nicolas, A., and F. Boudier, Mapping oceanic ridge segments in Oman ophiolites, *J. Geophys. Res.*, *100*, 6179–6197, 1995.
- Nicolas, A., and N. Chistensen, Formation of anisotropy in upper mantle peridotites: A review, in *Composition, Structure, and Dynamics of Lithosphere-Asthenosphere Systems, Geodyn. Ser.*, vol. 16, edited by K. Fuchs and C. Froidevaux, pp. 111–123, AGU, Washington D.C., 1987.
- Nicolas, A., and J. F. Violette, Mantle flow at oceanic spreading centers: Models derived from ophiolites, *Tectonophysics*, *81*, 319–339, 1982.
- Parmentier, E. M., and J. Phipps Morgan, Spreading rate dependence of three-dimensional structure in oceanic spreading centres, *Nature*, *348*, 325–328, 1990.
- Rabinowicz, M., A. Nicolas, and J. L. Vigneresse, A rolling mill effect in asthenosphere beneath oceanic spreading centers, *Earth Planet. Sci. Lett.*, *67*, 97–108, 1984.
- Rabinowicz, M., G. Ceuleneer, and A. Nicolas, Melt segregation and flow in mantle diapirs below spreading centers: Evidence from the Oman ophiolite, *J. Geophys. Res.*, *92*, 3475–3486, 1987.
- Raitt, R. W., G. G. Shor Jr., T. J. G. Francis, and G. B. Morris, Anisotropy of the Pacific upper mantle, *J. Geophys. Res.*, *74*, 3095–3109, 1969.
- Spiegelman, M., and D. P. McKenzie, Simple 2-D models for melt extraction at mid-ocean ridges and island arcs, *Earth Planet. Sci. Lett.*, *83*, 137–152, 1987.
- Su, W., and R. Buck, Buoyancy effects on mantle flow under mid-ocean ridges, *J. Geophys. Res.*, *98*, 12,191–12,205, 1993.
- Tilton, G. R., C. A. Hopson, and J. E. Wright, Uranium-led isotopic ages of the Samail ophiolite, Oman, with applications to the Tethyan ocean, *J. Geophys. Res.*, *86*, 2763–2775, 1981.
- Toomey, D. R., W. S. D. Wilcock, S. C. Solomon, W. C. Hammond, and J. A. Orcutt, Mantle seismic structure beneath the MELT region of the East Pacific Rise from P and S wave tomography, *Science*, *280*, 1224–1227, 1998.
- Wang, X. J., J. R. Cochran, and G. A. Barth, Gravity anomalies, crustal thickness, and the pattern of mantle flow at the fast spreading East Pacific Rise, 9 degrees-10 degrees N: Evidence for three-dimensional upwelling, *J. Geophys. Res.*, *101*, 17,927–17,940, 1996.
- Whitehead, J. A. J., H. J. B. Dick, and H. Schouten, A mechanism for magmatic accretion under spreading centres, *Nature*, *312*, 146–148, 1984.